

FIG. 2. Pattern diagrams of loading process

### 3. RESULTS OF TESTS

#### 3.1 Definition of a small resistance

Figure 3 shows the relationship between the shear stress and shear strain in Test-1 to Test-5. According to this, it is found that larger the maximum shear strain was, larger the shear strain needed to recover the strength was. And, it is also found that the relationships between the shear stress and the shear strain after the small resistance area were almost the same to each test.

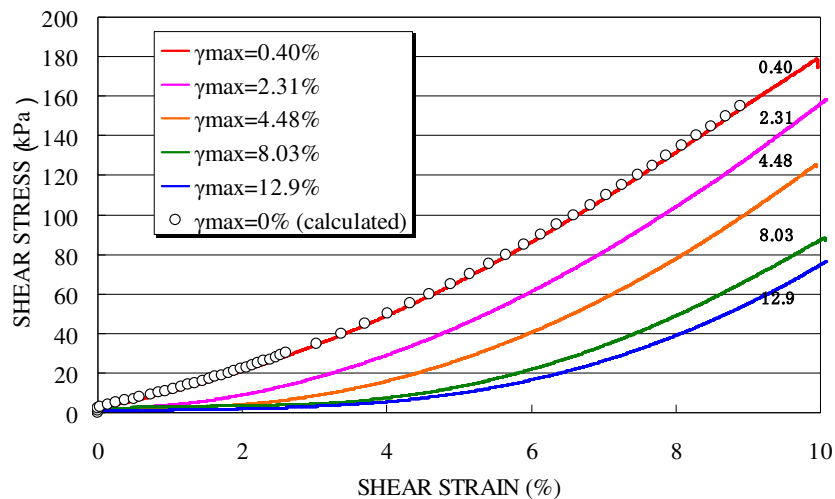
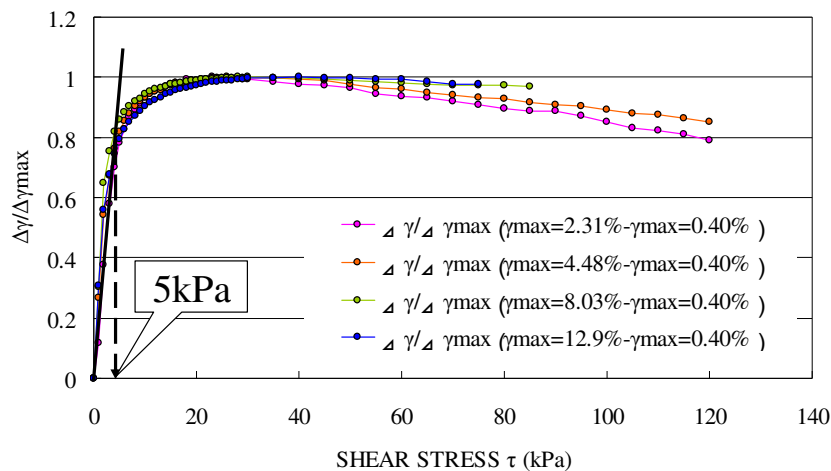


FIG. 3. Relationships between the shear stress and the shear strain

When the ground liquefaction was caused during an earthquake, the reason why a large deformation of ground was caused is mainly by the decreasing of strength in the small resistance area. So it is very important to evaluate this small resistance area. But the definition of this is not cleared as mentioned above. Therefore the small resistance area is defined as the shear strain which the shear strength increases to a certain level in this paper. The relationships between the maximum shear strain and the shear strain at same shear stress were calculated from FIG. 3 and the relationships between the shear stress and the shear strain at the maximum shear strain  $\gamma_{max}$  becomes 0% were calculated as shown in FIG. 3. It is found that the stress - strain curve at  $\gamma_{max} = 0$  kPa is almost the same as the curve at  $\gamma_{max} = 0.40$  %.

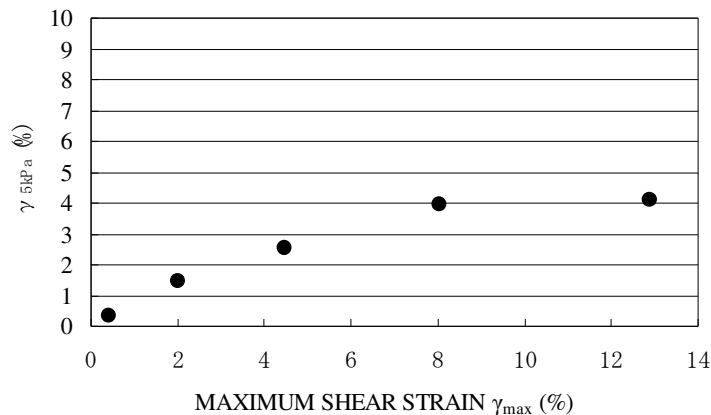
Based on the curve at  $\gamma_{max} = 0.40$  %, the difference of the shear strains in each case from the curve at  $\gamma_{max} = 0.40$  %,  $\Delta\gamma$ , was calculated. The relationships between  $\Delta\gamma/\Delta\gamma_{max}$  and the shear stress were shown in FIG. 4. Here  $\Delta\gamma_{max}$  is defined as the maximum  $\Delta\gamma$  in each case.



**FIG. 4. Relationships between  $\Delta\gamma/\Delta\gamma_{max}$  and Shear stress**

According to this figure, the curves of  $\Delta\gamma/\Delta\gamma_{max}$  and shear stress in each case are almost the same. So the small resistance area is defined as the area that this relationship keeps linear and the shear stress at the small resistance area is smaller than 5 kPa.  $\gamma_{5kPa}$ , is defined as the maximum shear strain at shear stress is 5 kpa.

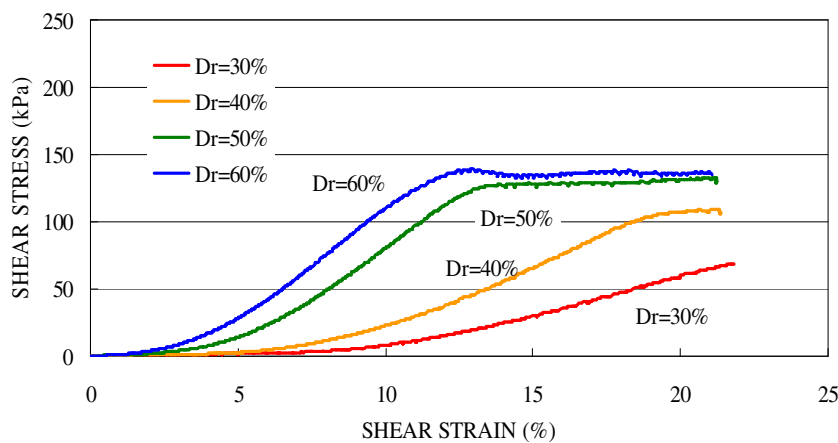
Figure 5 shows the relationships between the shear strains,  $\gamma_{5kPa}$  and the maximum shear strain,  $\gamma_{max}$ . It is found from this figure that larger the  $\gamma_{max}$  is, larger the  $\gamma_{5kPa}$  is. And the shear strain,  $\gamma_{5kPa}$ , increases linearly at the small  $\gamma_{max}$ . But the increase of  $\gamma_{5kPa}$  becomes smaller at large  $\gamma_{max}$  values.



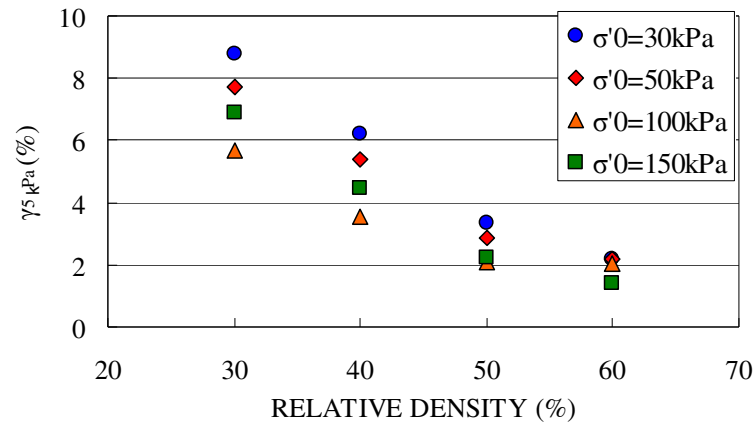
**FIG. 5. Relationships between  $\gamma_{5kPa}$  and  $\gamma_{max}$**

**3.2 Influence of the relative density and overburden pressure on the rigidity recovery process**

Figure 6 shows the relationships between the shear stress and the shear strain at the static loading process in the tests which initial effective stress is 30 kPa (Test-6, Test-10, Test-14 and Test-18). It is found that the stress-strain curve depends on the relative density and the shear strength at higher density is recovered faster than at the lower one. Larger shear strain is needed to recover the shear strength at lower density. Furthermore, the shear strength at the steady state depends also on the relative density. This tendency is observed in all cases from Test -6 to Test-21. Figure 7 shows the relationships between the relative density and  $\gamma_{5kPa}$ . It is also found that the influence of confining pressure becomes smaller at the higher density.

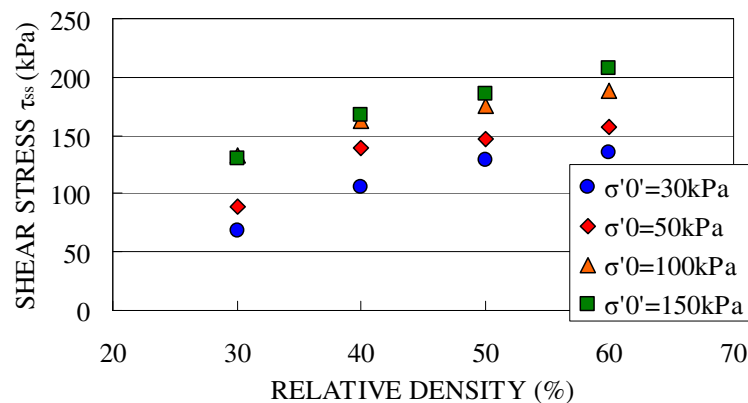


**FIG. 6. Relationships between the shear stress and the shear strain at  $\sigma'_o = 30$  kPa**



**FIG. 7. Relationships between the relative density and  $\gamma_{5kPa}$**

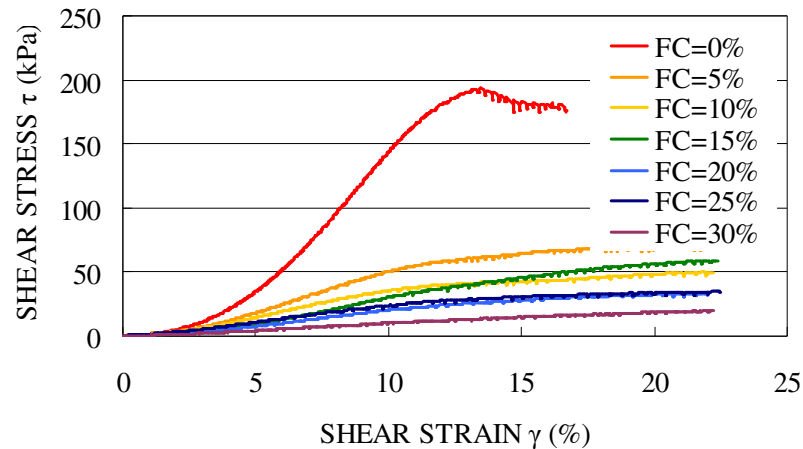
Figure 8 shows the relationships between the shear stress at the steady state  $\tau_{ss}$  and the relative density. It is clear that the shear stress  $\tau_{ss}$  depends on the relative density and the shear stress becomes larger in the higher relative density. The shear stress  $\tau_{ss}$  also depends on the overburden stress  $\sigma'_o$  but the shear stress  $\tau_{ss}$  at  $\sigma'_o = 100$  kPa is close to the one at  $\sigma'_o = 150$  kPa. The reason why the difference of the shear stress is caused is not clear yet. It is possible that the specimen of lower overburden pressure does not reach the steady state. But it is clear that the specimen of higher density reached to the steady state according to their shear stress – shear strain curve.



**FIG. 8. Relationships between the shear stress and the relative density**

### 3.3 Influence the fine fraction contents on the rigidity recovery process

Figure 9 shows that relationships between the shear stress and the shear strain in Test-24 to Test-29. To compare the results of silica sand, the results of Test-16 is also shown in FIG. 9. In these tests, the crushed stone powder was used as non plastic fine particles. According to this figure, the shear strain that needs to recover the shear stress becomes larger in the higher fine fraction contents.



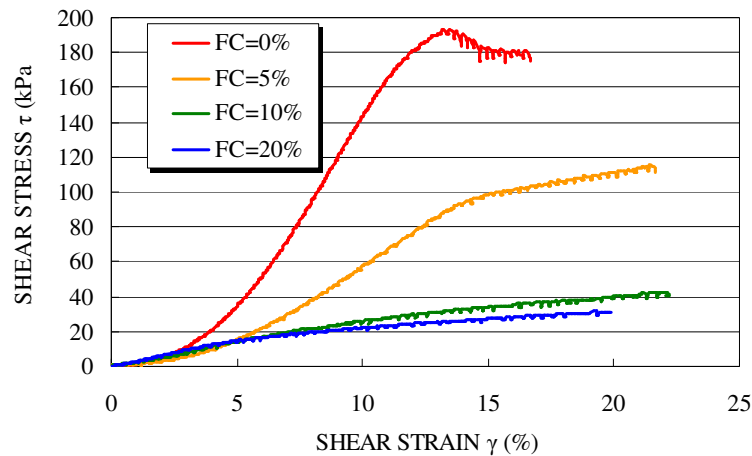
**FIG. 9. Relationships between the shear stress and the relative density**

Figure 10 shows the relationships between the shear stress and the shear strain in the case of Kibushi clay. Kibushi Clay is one of the cohesive clay. It is found from this figure that the specimen of FC =5% was recovered faster than the crushed stone powder. However in the case of FC =10 %, the relationship is the same to the one of crushed stone powder. In the area that the shear stress is small, it seems that the shear stress of the high fine fraction content is recovered quickly.

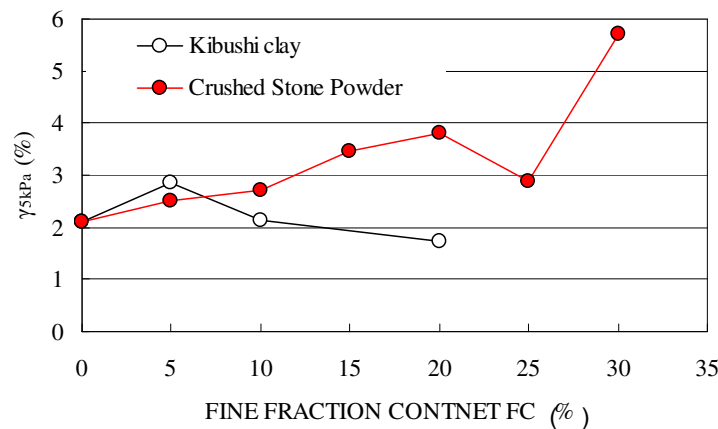
Two reasons of this are considerable. One is that fine particles spread the distance of particles and keep the void ratio in the specimen widely. So fine particles keep the relative density be small. The other is that the fine particles keep the soil structure be strong. It seems that the reason of that difference between the non plastic particle and the cohesion clay is latter. Furthermore the influence of the soil structure becomes smaller in the case of high fine fraction content (FC = 10% or 20%) and characteristics of fine particles become predominant. The reason of the quick recovery in the high fine fraction content is considered that the characteristics of fine particles become predominant.

Figure 11 shows the relationships between the small resistance area,  $\gamma_{5kPa}$  and the fine fraction contents FC. From this figure, it is found that the small resistance area with the crushed stone powder,  $\gamma_{5kPa}$  become larger than without the fine particles. However the small resistance area with the cohesion clay, Kibushi clay, does not become large. The reason of this is considered as follows. The specimen with the cohesion clay can keep its stiffness. Therefore the influence of disturbance of soil

structure becomes smaller and the influence of increase of void ratio becomes smaller. Even if the FC is increased, the small resistance area does not become large because these two influences are counterbalanced.



**FIG. 10. Relationships between the shear stress and the shear strain**



**FIG. 11. Relationships between  $\gamma_{5kPa}$  and the fine fraction content**

Figure 12 shows the relationship between the shear stress at the steady state,  $\tau_{ss}$  and the fine fraction content FC. It is also clear that the shear strength with the fine particles becomes small. The shear stress in the case of low FC sand becomes small linearly; however the trend of the reducing of the shear stress becomes gentle in the case of high FC sand. It implies that the fine particles have an influence on the rigidity recovery process when the soil structure is influenced by the fine particles.

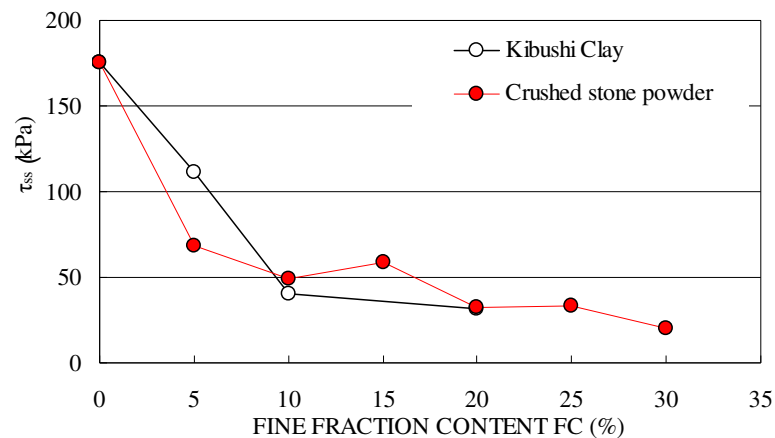


**FIG. 12. Relationships between the shear stress  $\tau_{ss}$  and the fine fraction content**

#### 4. CONCLUSIONS

This study aims to clarify the effects of some factors on the rigidity recovery of post liquefied soil. This paper describes results of a series of torsional hollow cylinder shearing tests to evaluate the shear stress – shear strain relationship of liquefied soil. Effects of fine fraction content, relative density, overburden pressure, and maximum shear strain during the shaking were discussed. Results revealed the following:

- 1) The rigidity recovery process is influenced by the maximum shear strain when the maximum shear strain is less than 8%.
- 2) It is also found that the recovery process is influenced by the relative density and the degree of influence is larger in the case of lower relative density.
- 3) The overburden pressure has also an influence on the rigidity recovery process.
- 4) The rigidity recovery process is influenced by the fine fraction content, FC. But the small resistance area of the sand with the cohesion clay is almost constant. Furthermore, the degree of the influence depends on the FC and when the FC is larger than 10%, the influence is small.

#### REFERENCES

- Yasuda, S., Masuda, T., Kiku, H and Itafuji, S. (1993). "Several torsional shear tests on deformation characteristics of soil before and after liquefaction," *Proceedings of the 28<sup>th</sup> Japan national conference on soil mechanics and foundation engineering*, JGS, 929-930.

## The Seismic Dilatometer Marchetti Test (SDMT) for Evaluating Liquefaction Potential Under Cyclic Loading

S. Grasso<sup>1</sup> and M. Maugeri<sup>2</sup>

<sup>1</sup> Ph. D. in Geotechnical Engineering, University of Catania, Faculty of Engineering, Viale Andrea Doria n. 6, 95125 Catania (Italy).

<sup>2</sup> Full Professor in Geotechnical Engineering, University of Catania, Faculty of Engineering, Viale Andrea Doria n. 6, 95125 Catania (Italy).

**ABSTRACT:** This paper presents a  $K_D$ -CRR corrected relation for sandy soils potential liquefaction evaluation under cyclic loading, on the basis of previous tentative CRR- $K_D$  curves proposed. The new tentative correlation for evaluating CRR from  $K_D$ , was formulated by combining previous CRR- $K_D$  correlations with the vast experience incorporated in current methods based on CPT and SPT for the evaluation of liquefaction potential. The Seismic Dilatometer Marchetti Test (SDMT) has the advantage, in comparison with CPT and SPT tests, to measure independent parameters, such as the Horizontal Stress Index ( $K_D$ ). A re-evaluation of CRR- $K_D$  correlation has been also made taking into account the numerous recent SDMT. The results show that the Horizontal Stress Index ( $K_D$ ) is a key-parameter and is very sensitive to potential liquefaction behaviour under cyclic loading. The plotted correlation with critical values of  $K_D$  is very simple to use for detecting liquefaction potential of soils.

CPT, SPT and SDMT data have been then used in the evaluation of the potential liquefaction at San Giuseppe La Rena site in Catania (Sicily, Italy), which is recognized as a typical Mediterranean city at high seismic risk.

### INTRODUCTION

The Seismic Dilatometer Marchetti Test (SDMT) is gradually entering into use in routine geotechnical investigations, allowing therefore the accumulation of numerous data. The SDMT provides, among other measurements, a parameter that previous experience indicated as bearing a significant relationship with soil liquefaction. Such parameter is the Horizontal Stress Index ( $K_D$ ), whose relationship with CRR has been illustrated by several authors (Monaco et al., 2005; Grasso and Maugeri, 2006). The Authors have collected in the recent years a large amount of measurements of  $K_D$  using SDMT in different sandy soils.

The coastal plain of the city of Catania (Sicily, Italy), which is recognized as a typical Mediterranean city at high seismic risk, was investigated by Seismic Dilatometer Marchetti Test (SDMT). Seismic liquefaction phenomena were reported by historical

sources following the 1693 ( $M_s = 7.0-7.3$ ,  $I_o = X-XI$  MCS) and 1818 ( $M_s = 6.2$ ,  $I_o = IX$  MCS) Sicilian strong earthquakes. The most significant liquefaction features seem to have occurred in the Catania area, near Saint Giuseppe La Rena site, situated in the meioseismal region of both events. These effects are significant for the implications on hazard assessment mainly for the alluvial flood plain just south of the city, where most industry and facilities are located.

In the site No.11 (Saint Giuseppe La Rena site) eight borings (No. 418÷425 of the database) were made and for all of them SPT data are available. Near the borings eleven CPT (No. 1÷11) tests were also made. The subsoil exploration revealed the presence of a sand with a content of fine particles less than 30% for a depth of about 10 meters.

For a new commercial building, deep site investigations have been performed, which included borings, SPT and CPT. More recently, at the same site, SDMT has been performed. The locations of the SPT, CPT and SDMT are reported in Fig. 1. SPT and CPT were located in the area where the commercial building has been built. The SDMT was performed after the construction of the building, and was located outside the construction area.

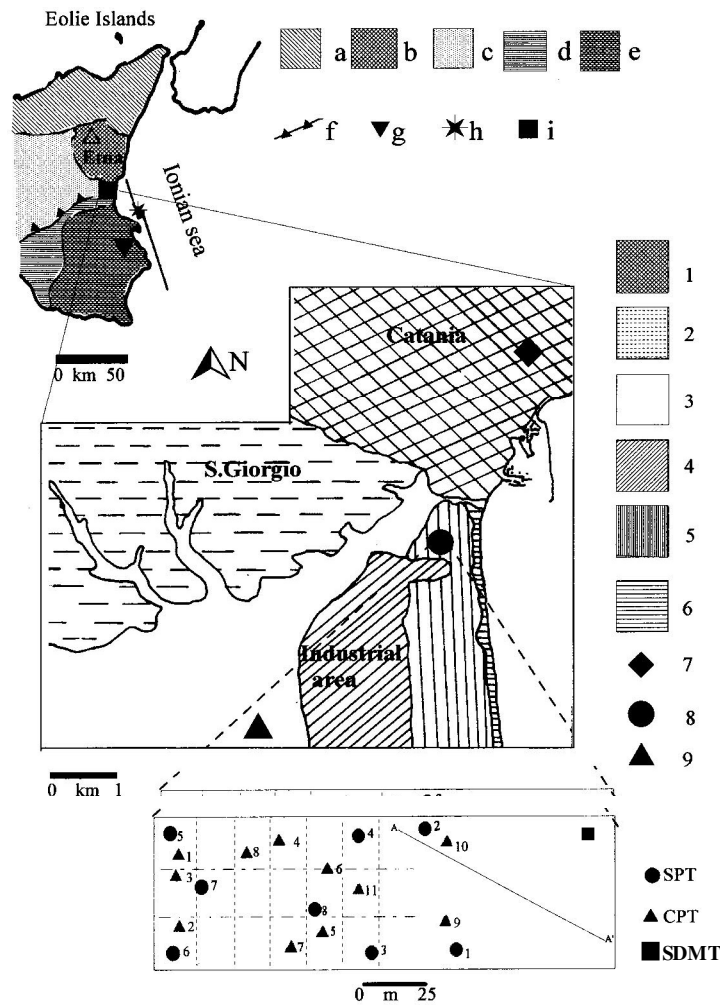


FIG. 1. Location of SPT, CPT and SDMT tests.

## CYCLIC SHEAR STRESS RATIOS INDUCED BY EARTHQUAKE GROUND MOTIONS

During cyclic undrained loading, like those imposed by earthquake shaking, almost all saturated cohesionless soils are subjected to significant pore pressure build-up due to the contractive response of the soil at low strain levels. If there is shear stress reversal, the effective stress state can drop rapidly to zero. When a soil element reaches the condition of essentially zero effective stress, the soil has very little stiffness and large deformations can develop during cyclic loading. This phenomenon is generally referred to as liquefaction.

The susceptibility of a site to seismic-induced liquefaction may be assessed comparing the cyclic soil resistance to the cyclic shear stresses due to the ground motion. The latter is of course a function of the design earthquake parameters, while the former depends on the soil shear strength and can be computed using results from in situ tests. The traditional procedure, introduced by Seed & Idriss (1971), has been applied for evaluating the liquefaction resistance of San Giuseppe La Rena sandy soil. This method requires the calculation of the cyclic stress ratio CSR, and cyclic resistance ratio CRR. If CSR is greater than CRR, liquefaction can occur.

The cyclic stress ratio CSR is calculated by the following equation (Seed & Idriss 1971):

$$CSR = \tau_{av} / \sigma'_{vo} = 0.65 (a_{max} / g) (\sigma_{vo} / \sigma'_{vo}) r_d / MSF$$

where  $\tau_{av}$  = average cyclic shear stress,  $a_{max}$  = peak horizontal acceleration at the ground surface generated by the earthquake,  $g$  = acceleration of gravity,  $\sigma_{vo}$  and  $\sigma'_{vo}$  = total and effective overburden stresses,  $r_d$  = stress reduction coefficient depending on depth and MSF is magnitude scaling factor. Seed and Idriss (1971) introduced the stress reduction coefficient  $r_d$  as a parameter describing the ratio of cyclic stresses for a flexible soil column to the cyclic stresses for a rigid soil column.

As the shear stresses induced at any point in a level soil deposit during an earthquake are primarily due to the vertical propagation of shear waves in the deposit, these stresses can be calculated using analytical procedures and are particularly dependent on the earthquake ground motion characteristics (e.g., intensity and frequency content), the shear wave velocity profile of the site, and the dynamic soil properties (Idriss and Boulanger, 2004). So, the parameter  $C$  could be adequately expressed as a function of depth and earthquake magnitude ( $M$ ) as reported in Idriss (1999), in extending the work of Golesorkhi (1989):

$$\ln(r_d) = \alpha(z) + \beta(z)M$$

$$\alpha(z) = -1.012 - 1.126 \sin(z/11.73 + 5.133)$$

$$\beta(z) = 0.106 + 0.118 \sin(z/11.28 + 5.142)$$

in which  $z$  is depth in meters and  $M$  is moment magnitude. These equations are considered appropriate to a depth  $z \leq 34$  m. Plots of  $r_d$  calculated using previous equation for  $M = 5\frac{1}{2}$ ,  $6\frac{1}{2}$ ,  $7\frac{1}{2}$  and 8 are presented in Figure 2. Also shown in this figure is the average of the range published by Seed and Idriss in 1971.